Published in final edited form as:
J Pharmacol Exp Ther. 2008 July ; 326(1): 296–305. doi:10.1124/jpet.107.135863.

Impact of Impurity on Kinetic Estimates from Transport and Inhibition Studies

Pablo González and **James E. Polli**
Department of Pharmaceutical Sciences, School of Pharmacy, University of Maryland, Baltimore, Maryland (P.G., J.E.P.); and Departamento de Farmacia, Facultad de Química, Pontificia Universidad Católica de Chile, Santiago, Chile. (P.G.)

Abstract

Although in vitro transport/inhibition studies are commonly performed on impure drug candidates to screen for pharmacokinetic properties in early development, quantitative guidelines concerning acceptable impurity levels are lacking. The broad goal was to derive models for the effect of impurity on transport and inhibition studies and identify the maximum allowable impurity level that does not bias assay results. Models were derived and simulations performed to assess the impact of impurity on substrate properties K_t and J_{max} and inhibition K_i. Simulation results were experimentally challenged with known amount of impurity, using the intestinal bile acid transporter as a model system. For substrate uptake studies, glycocholate served as substrate and was contaminated with either a very strong, strong, or moderate impurity (i.e. taurolithocholate, chenodeoxycholate, or ursodeoxycholate, respectively). For inhibition studies, taurocholate and glycocholate was the substrate/inhibitor pair, where glycocholate was contaminated with taurolithocholate. There was high agreement between simulation results and experimental observations. Not surprisingly, in the inhibition assay, potent impurity caused test compound to appear more potent than the test compound's true potency (i.e. reduced inhibitory K_i). However, results in the transport scenario surprisingly indicated that potent impurity did not diminish test compound potency, but rather increased substrate potency (i.e. reduced Michaelis-Menten substrate K_t). In general, less than 2.5% impurity is a reasonable target, provided the impurity is less than 10-fold more potent than test compound. Study results indicate that careful consideration of possible impurity effect is needed when QSAR analysis cannot explain high compound potency from transport or inhibition studies.

INTRODUCTION

Transport and inhibition studies are routinely performed in early development to screen for absorption, distribution, metabolism and excretion (ADME). For example, a current project in our laboratory concerns the targeting of an intestinal transporter for drug delivery purposes (Balakrishnan and Polli, 2006). The transporter is the human Apical Sodium-dependent Bile Acid Transporter (hASBT). ADME considerations in this project motivate the screening for substrates and inhibitors of hASBT, in order to construct a quantitative structure-activity relationship (QSAR) model for inhibitors and substrates of this transporter. Test compounds are currently being synthesized to evaluate the chemical structural features that allows for hASBT inhibition, as well as translocation by hASBT (Balakrishnan et al., 2006a).

However, test compounds in early development often contain chemical impurities, including intermediates that bear structural similarity to the target test compound. The presence of such

Corresponding Author: James E. Polli, Department of Pharmaceutical Sciences, School of Pharmacy, University of Maryland, 20 Penn Street, HSF2 room 623, Baltimore, MD 21201 Telephone: 410-706-8292Fax: 410-706-5017 jpolli@rx.umaryland.edu.

impurities has potential to affect the results of pharmacologic assays, including ADME screening results. The Journal of Pharmacology and Experimental Therapeutics does not provide guidelines about compound purity. Since January 2007, the Journal of Medicinal Chemistry now requires that key target compounds possess purity of 98% or more. However, well developed guidelines and their rationale about acceptable level of impurity, based upon possible impurity impact on assay results during early development, are surprisingly lacking. Guidance on impurity effects on ADME screening studies would be helpful.

The present study concerns two types of ADME transport studies: inhibition studies and transport/uptake studies. Presumably, in a competitive binding study (e.g. inhibition study), impurity with a potency greater than test compound potency may cause test compound to appear more potent than actually is. This expectation was found to be correct here and quantitative guidelines are provided. Surprisingly, an expectation that a potent impurity would diminish the apparent potency of a test compound in the uptake assay (i.e. increase Michaelis-Menten K_t) was found here to be incorrect. Rather, potent impurity, which reduces test compound flux, resulted in test compound to appear to possess higher substrate affinity (i.e. exhibit a lower K_t). This study provides quantitative guidelines, which are currently lacking, about maximum impurity levels to avoid bias on transporter parameter estimates (i.e. K_t, J_{max}, and K_i) in early drug discovery. Results have implications for other types of early discover assays, such as pharmacologic binding studies.

METHODS

Overall Study Design

Both simulation studies and experimental studies were performed, for both transport/uptake studies, as well as inhibition studies. Table 1 summarizes the four types of studies. In transport/uptake studies, the impurity is a contaminant of the substrate. Simulation studies were conducted over a wide range of conditions. The experimental uptake studies employed taurolithocholic acid (TLCA), chenodeoxycholic acid (CDCA), and ursodeoxycholic acid (UDCA) as very strong, strong, and moderate potent impurities, respectively. In inhibition studies, the impurity is a contaminant of the inhibitor.

Materials

[^{3}H]-Taurocholic acid (10 μCi/mmol) and [^{14}C]-glycocholic acid (55 mCi/mmol) were purchased from American Radiolabeled Chemicals, Inc, (St. Louis, MO). Taurocholic acid (TCA), glycocholic acid (GCA), taurolithocholic acid TLCA, and ursodeoxycholic acid UDCA were from Sigma Aldrich (St. Louis, MO). CDCA was obtained from TCI America (Portland, OR). Geneticin, fetal bovine serum (FBS), trypsin, and DMEM were purchased from Invitrogen (Rockville, MD). All other reagents and chemicals were of the highest purity commercially available.

Cell Culture

Stably-transfected hASBT-MDCK cells were cultured as previously described (Balakrishnan et al., 2005). Briefly, cells were grown at 37 °C, 90% relative humidity, 5% CO_2 atmosphere and fed every 2 days. Culture media consisted on DMEM supplemented with 10% FBS, 50 units/mL penicillin, and 50 μg/mL streptomycin. Geneticin was added at 1 mg/mL to maintain selection pressure. Cells were passaged after 4 days or after reaching 90% confluency.

Uptake Studies

Uptake studies were performed to obtain kinetic parameters that relate to compound binding and subsequent translocation into the cell monolayer. Stably-transfected hASBT-MDCK cells

were grown on 12-well plates (3.8 cm^2, Corning, Corning, NY) and grown under conditions described above. Briefly, cells were seeded at a density of 1.5 million/well and induced with 10 mM sodium butyrate 12–15 h at 37 °C prior to study on day 4. Cells were washed thrice with Hank's balanced salt solution (HBSS) or modified HBSS prior to uptake assay. Studies were conducted at 37 °C, 50 rpm for 10 min in an orbital shaker. Uptake buffer consisted of either HBSS, which contains 137 mM NaCl, or a sodium-free, modified HBSS where NaCl was replaced by 137 mM tetraethylammonium chloride (pH 6.8). Since ASBT is sodium dependent, studies using sodium-free buffer allowed for the measurement of passive uptake. Kinetics of hASBT-mediated GCA uptake (n=3) was assessed at different donor concentrations (1–200 μM spiked with 0.2 μCi/mL of [^{14}C]-GCA), in presence and absence of impurity. When impurity was present, each GCA donor solution was contaminated with TLCA, CDCA, or UDCA (i.e. impurity) to yield a mole fraction of impurity, X_i, of 2, 4, 6, 8, and 10%, respectively. K_i of these impurities was obtained from GCA-uptake inhibition studies (see below).

At the end of the assay, active uptake was stopped by washing the cells thrice with chilled sodium-free buffer. Cells were then lysed with 0.25 mL of 1 N NaOH overnight, allowing for complete evaporation, and reconstituted with 0.50 mL of 0.5 N HCl. Cell lysate was counted for associated radioactivity using an LS6500 liquid scintillation counter (Beckmann Instruments, Inc., Fullerton, CA).

Inhibition Assay

To characterize hASBT binding affinities, cis-inhibition studies of TCA or GCA uptake were conducted as described. Cells were exposed to donor solutions containing relevant substrate (2.5 μM TCA + 0.5 μCi/ml [^{3}H]-TCA or 5 μM GCA + 0.2 μCi/mL [^{14}C]-GCA) and inhibitor (1–200 μM) for 10 min. GCA inhibition of TCA was measured in absence and presence of impurity. When impurity was present, each GCA donor solution was contaminated with TLCA (i.e. impurity) to yield a mole fraction of impurity, X_j, of 2, 4, 6, 8, and 10 %, respectively. TLCA inhibition of TCA uptake was also measured to obtain K_j (see below). After 10 min, donor solution was removed, cells washed three times with chilled sodium-free buffer, lysed, and counted for associated radioactivity (i.e TCA). Inhibition data were analyzed in terms of inhibition constant K_i as described below.

Simulation of Substrate Transport: Impurity Effect on Substrate Flux

To assess the impact of impurity on substrate flux, simulations were performed using eqn 1 and 2 (appendix A) for scenarios with and without impurity, respectively. Equations 1 and 2 are denoted the impurity-present model and the impurity-absent model, respectively, for transport/uptake studies.

$$J_{X_i} = \frac{P_{ABL} \cdot \left(\frac{J_{\max}}{K_t\left(1+\frac{\left(\frac{X_i \cdot S}{1-X_i}\right)}{K_i}\right)+S} + P_p \right)}{P_{ABL} + \frac{J_{\max}}{K_t\left(1+\frac{\left(\frac{X_i \cdot S}{1-X_i}\right)}{K_i}\right)+S} + P_p} \cdot S \quad (1)$$

$$J = \frac{P_{ABL} \cdot \left(\frac{J_{max}}{K_t + S} + P_p\right)}{P_{ABL} + \frac{J_{max}}{K_t + S} + P_p} \cdot S \quad (2)$$

Flux in the presence of impurity (J_{Xi}) was calculated using eqn 1 over a range of K_t, X_i and K_i values. Substrate K_t was 5, 50, and 500 μM; substrate concentration (S) was 1/10 of K_t. Impurity level (X_i) was varied from 0 to 10% mole fraction, with greater sampling for larger K_t scenarios. K_i was 0.05, 0.5, 5, 50, and 500 μM, respectively. J_{max}, P_{ABL} and P_p were fixed to 0.5 pmol/cm^2/s, 70×10^{-6} cm/s, and 0.5×10^{-6} cm/s, respectively, in all cases (Balakrishnan et al., 2007). Eqn 2 (i.e. flux without impurity, J) is eqn 1 when $X_i = 0$. The ratio J_{Xi}/J was calculated as a metric for impurity effect on flux and plotted against X_i. It is important to note that S was the actual assigned substrate concentration in donor; the concentration of substrate and impurity (when $X_i > 0$) was greater than S.

Simulation of Substrate Transport: Impurity Effect on K_t and J_{max} Estimates

To assess impurity effect on K_t and J_{max} estimates from transport studies, simulated flux data was generated from impurity-present model (eqn 1). Across the simulations, K_t was 5, 50, or 500 μM, while J_{max} was 0.5 pmol/cm^2/s. Since the aim of these simulation studies is to measure impurity effect on bias on estimated K_t and J_{max} parameter fits, these K_t values (i.e. 5, 50, and 500 μM) and J_{max} value (i.e. 0.5 pmol/cm^2/s) are denoted as "true K_t" and "true J_{max}", respectively. In simulations, S was 1/20, 1/10, 1/5, ½, 1, 2, 5, 10 and 20 times K_t to assure saturation of active transport. P_{ABL} and P_p were 70×10^{-6} cm/s and 0.5×10^{-6} cm/s, respectively. Simulated flux data was subsequently fitted to impurity-absent model (eqn 2), for each unique condition (i.e. unique K_t, K_i, and X_i scenario). Nonlinear regression was used to simultaneously estimate K_t and J_{max} using SigmaPlot 8.0 (SPSS®Inc; Chicago, IL). In all cases, $r^2 = 1.000$. Results are discussed in terms of resulting bias in K_t and J_{max}, due to impurity, relative to "true K_t" and "true J_{max}" values that were employed in simulating flux data. K_t estimates were plotted against impurity level for each "true K_i" level. Similar plots were graphed for J_{max} estimates. Estimation error in K_t (or J_{max}) that exceeded 20% was considered unacceptably biased.

Simulation of Inhibition Studies: Impurity Effect on K_i Estimate

To simulate impurity influence on K_i estimate, eqn 3 (appendix B) was used to simulate inhibition profiles, where inhibitor was contaminated with impurity. Equation 3 is the impurity-present inhibition model.

$$J_{X_j} = \frac{P_{ABL} \cdot \left(\frac{J_{max}}{K_t\left(1 + \frac{I}{K_i} + \frac{\left(\frac{X_j \cdot I}{1 - X_j}\right)}{K_j}\right) + S} + P_p\right)}{P_{ABL} + \frac{J_{max}}{K_t\left(1 + \frac{I}{K_i} + \frac{\left(\frac{X_j \cdot I}{1 - X_j}\right)}{K_j}\right) + S} + P_p} \cdot S \quad (3)$$

It should be noted that, in contrast to transport simulations above where K_i is the inhibition constant of the impurity that contaminates the substrate, here K_i is the unbiased inhibition constant of the inhibitor (i.e. the value to be measured in the inhibition study). K_j is the unbiased inhibition constant of the impurity that contaminates the inhibitor. Impurity is present in

inhibitor at level X_j. Across simulations, K_t, J_{max}, P_{ABL} and P_p were fixed to be 5 μM, 0.5 pmol/cm^2/s, 70 × 10^{-6} cm/s and 0.5 × 10^{-6} cm/s, respectively, which reflects active TCA transport across hASBT-MDCK monolayers (Balakrishnan et al., 2007) K_i was 0.05, 0.5, 5, 50, and 500 μM. Inhibitor concentration was 1/20, 1/10, 1/5, ½,1, 2, 5, 10, and 20 times K_i. Impurity K_j was 0.5, 5, and 50 μM. An entire inhibition profile was generated for each level of impurity (X_j), which ranged from 0 to 10% mole fraction. Each inhibition profile (i.e. unique K_i, K_j, and X_j scenario) was fitted to impurity-absent inhibition model (eqn 4, appendix B) using nonlinear regression. Only K_i was estimated, while all other parameters assumed their true values. In all cases, $r^2 = 1.000$, except for one extreme inhibition study simulation (K_i = 500 μM) where $r^2 < 0.6$.

$$J = \frac{P_{ABL} \cdot \left(\frac{J_{max}}{K_t\left(1+\frac{I}{K_i}\right)+S} + P_p \right)}{P_{ABL} + \frac{J_{max}}{K_t\left(1+\frac{I}{K_i}\right)+S} + P_p} \cdot S \tag{4}$$

Results are discussed in terms of resulting bias in K_i, due to impurity, relative to "true K_i" values that were employed in simulating inhibition profile. K_i estimates were plotted against impurity level for each "true K_j" level. Estimation error in K_i that exceeded 20% was considered unacceptable bias.

Impurity Effect on Active Uptake Kinetic Estimates: Experimental Evidence

A series of uptake experiments where model substrate GCA was contaminated with model impurities TLCA, CDCA or UDCA were conducted in order to confirm simulation predictions. These bile acids were selected for several reasons. Previous data from our laboratory have shown GCA K_t to be 11.0 ± 1.9 μM. K_i for TLCA, CDCA, and UDCA were 0.50 ± 0.05 μM, 1.94 ± 0.17 μM, and 22.6 ± 3.0 μM, respectively (Balakrishnan et al., 2006b). TLCA, CDCA, and UDCA were chosen as impurities due to their high structural similarity to the substrate probe (i.e. GCA) and since they represent cases were $K_t/K_i \approx 100$, 10, and 1, respectively.

The uptake format was chosen to keep P_p at a minimum since high passive permeability (i.e. low monolayer integrity on transport format) was found to hinder proper evaluation of impurity impact on active transport parameter estimates. For uptake studies, P_{ABL} was set to 1.5 × 10^{-4} cm^2/s in analyzing experimental data (Balakrishnan et al., 2007). Since the impurity-present uptake and inhibition models are based on the assumption of competitive inhibition between the compound of interest and the impurity, a Dixon's analysis was performed to investigate the inhibition mechanism of TLCA on GCA uptake.

Analysis of Experimental Data from Uptake Studies

Experimental data from GCA uptake studies (X_i = 0–10%, with and without sodium), and from impurity-mediated inhibition of GCA uptake were combined and fitted simultaneously to eqn 1, 2, 4, and 5 in WinNonlin 5.2 (Pharsight, Mountain View, CA) using nonlinear regression to obtain "unbiased" estimates of GCA K_t, J_{max}, K_i, and P_p. Subsequently, values of these "unbiased" estimates were applied to eqn 1 (i.e. impurity-present uptake model) to simulate GCA uptake profiles when X_i was 2, 4, 6, 8, and 10 %, respectively. Predicted "biased" K_t and J_{max} were obtained by nonlinear fitting of these subsequent curves to eqn 2.

$$J = \frac{P_{ABL} \cdot P_p \cdot S}{P_{ABL} + P_p} \quad (5)$$

In order to challenge the predictive accuracy of the impurity-present model, GCA uptake in presence of impurity was fitted to eqn 2 (i.e. impurity-absent uptake model) to obtain observed "biased" GCA kinetic estimates K_t and J_{max} for each level of impurity mole fraction, X_i. Predicted bias and observed bias were compared.

Analysis of Experimental Data from Inhibition Studies

Compared to data analysis of uptake studies, the same approach was taken to challenge the impurity-present inhibition model and analyze impurity effect on GCA K_i. GCA inhibition of TCA uptake (with and without TLCA as impurity) and TLCA inhibition profile were fitted simultaneously to eqns 3 and 4, respectively, using nonlinear regression to obtain "unbiased" estimates of K_i, K_j, J_{max}, and P_p. TCA K_t was obtained from parallel uptake studies. Subsequently, values of these "unbiased" estimates were applied to eqn 3 (i.e. impurity-present inhibition model) to simulate GCA inhibition profiles when X_j was 2, 4, 6, 8, and 10 %, respectively. Predicted "biased" K_i was obtained by nonlinear fitting of these curves to eqn 4.

In order to challenge the predictive accuracy of the impurity-present inhibition model, GCA inhibition studies in presence of impurity were fitted to eqn 4 (impurity-absent inhibition model) to obtain observed "biased" GCA K_i for each level of impurity mole fraction, X_j. Predicted bias and observed bias were compared.

RESULTS

Simulation results are presented first, followed by supporting experimental observations (Table 1).

Simulation of Substrate Transport: Impurity Effect on Substrate Flux

Simulations indicate that impurity generally decreased substrate flux across cell monolayers. For example, Fig. 1 illustrates the decrease in flux of a moderate substrate (i.e. K_t = 50 μM) in the presence of increasing amount of impurity, particularly for the more potent impurities. A 20% decrease in flux was observed when the impurity was a strong inhibitor (i.e. K_i = 0.5 μM; open circles) and present at about 3.5% molar fraction level. Meanwhile, only a 0.5% mole fraction of a most strong inhibitor (i.e. K_i = 0.05 μM; closed circles) was needed to cause a 20% decrease in flux. Simulations covering a broader range of K_t values showed similar trends, including the susceptibility of weaker substrates to more pronounced impurity effects (see supplemental data Fig. a).

Figure 2 illustrates the effect of impurity potency on flux profile of a strong substrate (K_t = 5 μM). Impurity level was X_i = 2%. In general, greater inhibition potency of impurity resulted in reduced substrate flux. For example, a most strong impurity (K_i = 0.05 μM) reduced substrate flux about three-fold at 50 μM substrate concentration. Of note, an impurity whose K_i is equal to the substrate's K_t (i.e. K_i = 5 μM), had no marked effect. Meanwhile, the impurities with 10-fold (i.e. K_i = 0.5 μM) and 100-fold (i.e. 0.05 μM) greater potency provided notable flux reduction. Qualitatively similar results were observed for the effect of impurity potency on moderate (K_t = 50 μM) and weak (K_t = 500 μM) substrate (data not shown), although the effects are more dramatic.

Simulation of Substrate Transport: Impurity Effect on K_t and J_{max} Estimates

The impact of impurity on K_t and J_{max} was assessed by fitting simulated data from eqn 1 (i.e. impurity-present model) onto eqn 2 (i.e. impurity-absent model). This approach mimics the perhaps common scenario in early discovery where impurity is present but data analysis assumes no impurity. Bias in kinetic estimates was negative, to reduce the estimated values of K_t and J_{max}. While this effect in J_{max} is intuitive, this effect on K_t would appear to be unexpected. As described above, impurity reduced substrate flux, but resulted in the substrate to appear as a substrate with greater affinity than it truly possesses (i.e. estimated K_t < "true" K_t).

Figure 3 illustrates estimated K_t as a function of impurity level for a strong substrate (5 μM). Bias was deemed to occur when impurity caused more than a 20% error in estimate. From Fig. 3, the impurity potency needed to be at least 10-fold higher than that of the substrate to cause bias. When $K_t/K_i = 10$, the impurity level needed to cause bias was always about 2.5% mole fraction. For example, $X_i = 2.5\%$ lead the estimated K_t to be 4 μM when $K_t/K_i = 10$. Simulations covering a broader range of K_t values showed similar trends, including the susceptibility of weaker substrates to impurity effects (see supplemental data Fig. b)

Table 2 summarizes the relationship between K_t/K_i ratio and the necessary X_i to cause bias. In Table 2, regardless whether the potency of the substrate was 5 μM, 50 μM, or 500 μM, K_t/K_i ratio of 10 always resulted in K_t bias, although bias required the impurity level to be at least 2.5 % mole fraction. When $K_t/K_i = 100$, about 0.25% impurity caused 20% bias, depending on K_t value. However, when $K_t/K_i = 1$ or less, bias did not manifest for even $X_i = 10\%$.

Regarding effect of impurity on J_{max}, plots of estimated J_{max} versus X_i were identical to those in Fig 3. Interestingly, X_i levels had the same relative effect on J_{max} as on K_t (Supplemental data Fig. c). Although presented for impurity effect on K_t bias, Table 2 equally applies for J_{max} bias. For example, when $K_t/K_i = 1$ or less, bias in J_{max} did not manifest.

While the effect on J_{max} is intuitive, this effect of impurity to reduce K_t would appear to be unexpected. K_t is often interpreted as an affinity parameter, such that impurity effects would result in the substrate to appear as a substrate with greater affinity than it truly possesses (i.e. estimated K_t < "true" K_t). Figure 2 illustrates the basis for this effect. Figure 2 was generated for $X_i = 2\%$ for a strong substrate ($K_t = 5$ μM). For the scenario $K_i = 0.5$ μM (open circles), estimated J_{max} and K_t were 0.415 pmol/cm^2/s and 4.15 μM, respectively, which are each 17% less than "true" values of 0.5 pmol/cm^2/s and 5 μM, respectively. In this scenario, it can be interpreted than impurity effect to reduce J_{max} estimate causes a proportional effect on K_t estimate, vis-à-vis the J_{max} effect. Since K_t is the concentration at half J_{max}, and since impurity reduces apparent J_{max}, impurity reduces apparent K_t.

Simulation of Inhibition Studies: Impurity Effect on K_i Estimates

In addition to transport studies, inhibition studies are frequently performed in development and design to evaluate the ability of a compound to inhibit the transport of a known substrate. Data are often interpreted as an inhibition constant (K_i). Here, impurity J_{imp} contaminates inhibitor I and competes against I (and substrate) for the same transporter in a non-cooperative fashion (see Supplemental Data Fig. d). By virtue of impurity contributing additional inhibition, impurity can produce negative bias in K_i estimates from inhibition studies.

The extent of this bias is illustrated in Fig. 4 (substrate $K_t = 5$ μM) for a strong inhibitor ($K_i = 5$ μM) and shows bias depended on the affinity of the impurity (i.e. K_j) and its mole fraction, X_j. For example, a very strong impurity ($K_i = 5$ μM) at $X_i = 2.5\%$ caused 20% bias in estimated K_i, resulting in apparent K_i to be 4 μM. Simulations covering a broader range of K_i values showed similar trends, including the susceptibility of weaker inhibitors to more pronounced

impurity effects (see supplemental data Fig. e). The impact of impurities on inhibition results mimics the above effect on transport studies.

Table 3 summarizes the relationship between K_i/K_j ratio and the impurity level required to produce bias on K_i estimates. Results in Table 3 from inhibition studies mimic results in Table 2 from transport studies, although Table 3 concerns K_i/K_j ratio while Table 2 concerns K_t/K_i ratio. In Table 3, no bias manifested when $K_i/K_j \leq 1$, similar to an observation in Table 2. Also, for either a strong or moderate inhibitor, $K_i/K_j = 10$ resulted in bias when X_j was at least 2.5%, similar to an observation in Table 2. For a moderate inhibitor, $X_j = 0.6\%$ caused bias in K_i when $K_i/K_j = 100$.

Impurity Effect on Active Uptake Kinetic Estimates: Experimental Evidence

A series of uptake experiments where model substrate glycocholic acid (GCA) was contaminated with model impurities taurolithocholic acid (TLCA), chenodeoxycholic acid (CDCA) or ursodeoxycholic acid (UDCA). GCA K_t is about 10 μM, such that K_t/K_i for TLCA, CDCA, and UDCA were about 100, 10, and 1, respectively (Balakrishnan et al., 2006b). TLCA was found to be a competitive inhibitor of GCA uptake (Supplemental Data Fig. f).

Figure 5 shows bias on GCA K_t and J_{max} estimates from uptake when TLCA was present as impurity. These estimates were always negatively biased by presence of TLCA at the entire range of X_i studied. Unbiased K_t and J_{max} of substrate were 12.6 (±1.1) uM and 0.424 (±0.041) pmol/cm^2/s, while TLCA K_i was 0.11 (±0.01) uM. When $X_i = 2\%$ observed K_t and J_{max} estimates of GCA were 3.76 (±0.87) μM and 0.113 (±0.004) pmol/cm^2/s, representing an estimation error of 70 and 73% respectively. From Fig. 5A, interpolation predicts that a 0.24% mole fraction of TLCA would produced a 20% bias on GCA K_t estimate (experimental $K_{t\ GCA}/K_{i\ TLCA} = 114$) reflecting the high level of agreement between model predictions and observed results ($r^2 = 0.979$ for K_t and 0.995 for J_{max}).

Identical experiments were performed with GCA contaminated with CDCA as impurity. Unbiased GCA K_t and J_{max} were 11.0 (±1.8) μM and 0.153 (±0.013) pmol/cm^2/s respectively, while unbiased CDCA $K_i = 1.39$ (±0.39) μM ($K_t/K_i = 7.92$). While CDCA caused negative bias on GCA J_{max} regardless of impurity load, K_t estimates were biased only when $X_i > 2\%$. Figure 6 show the bias effect of CDCA on GCA K_t and J_{max}. Experimentally, a 6% mole fraction of CDCA caused a 20% drop on estimated GCA K_t relative to the unbiased value, while 4% caused similar estimation error on J_{max}. The ability of the model to predict biased K_t estimates was modest ($r^2 = 0.806$) and good to predict J_{max} ($r^2 = 0.908$).

Identical studies were also performed with GCA-UDCA as substrate-impurity pair. Unbiased GCA K_t was 9.82 (±0.79) μM. Unbiased UDCA K_i was 24.2 (±2.8) μM, such that $K_t/K_i = 0.40$ for this GCA-UDCA pair. Unlike the above GCA-TLCA and GCA-CDCA pairs, it was not possible to obtain biased estimates for the GCA-UDCA pair due to poor inhibitory potency of the UDCA impurity.

Impurity Effect on Inhibition Constant Estimates: Experimental Evidence

To evaluate the impact of impurity on K_i estimates from inhibition assays, GCA-mediated inhibition of taurocholic acid (TCA) uptake was measured in absence and presence of TLCA as impurity ($X_j = 0$–10%). X_j here represents the mole fraction of impurity J_{imp} (i.e. TLCA) contaminating inhibitor I (i.e. GCA) (Supplemental Data Fig. d). This inhibitor-impurity pair was chosen to represent a $K_i/K_j \approx 10$ based on previous data (Balakrishnan et al., 2006b). Figure 7 shows bias on GCA K_i estimates as a function of TLCA mole fraction. Unbiased GCA K_i was 5.05 (±0.48) μM, while unbiased TLCA K_j was 0.40 (±0.04) μM ($K_i/K_j = 12.6$). TLCA contamination caused negative bias on GCA inhibition constant estimation over the entire

range of X_j. For example, when TLCA was present at a 2% mole fraction, observed GCA K_i estimate was 4.39 (±0.32) μM. Interpolation of predicted data identified a critical X_j level of 1.95% to obtain a 20% bias on GCA K_i estimation. The impurity-present model predicted observed bias on K_i (r^2= 0.919).

DISCUSSION

Implications for ADME Screening and hASBT Studies

Transport and inhibition studies are routinely performed in early development to screen for ADME. A current project in our laboratory concerns the targeting of hASBT for drug delivery purposes (Balakrishnan and Polli, 2006). ADME considerations motivate the screening for substrates and inhibitors of hASBT, in order to construct a QSAR model for inhibitors and substrates of this transporter.

hASBT (SLC10A2) is a 348 aminoacid transmembrane protein that mediates the active uptake of bile acids in the small intestine playing a critical role in the bile acid enterohepatic recirculation (Hagenbuch and Dawson, 2004). The total bile acid pool in humans (3–5 g) recirculates several times a day giving a turnover of 12–18 g/day (Hofmann, 1999). However, no more than 0.5 g are lost in the feces daily, reflecting the high capacity and efficiency of this transporter (Hofmann and Mysels, 1992). This suggests that some drugs with poor oral absorption may benefit from conjugation to bile acids by utilizing hASBT as carrier to enter the enterocyte. Despite the enormous potential of hASBT as target for bile acid containing prodrugs, only a few examples of its use can be found in the literature (Sievanen, 2007). Employing this approach, the oral bioavailability of acyclovir was enhanced in rats via a bile acid conjugate prodrug of acyclovir (Tolle-Sander et al., 2004). Also, hASBT is a promising pharmacological target, where hASBT inhibitors could lower blood cholesterol (Buchwald et al., 2002). Hence, hASBT is a target for novel substrates and inhibitors. An understanding of impurity effects on transport and inhibition assays is needed and the subject of this report.

Since January 2007, the Journal of Medicinal Chemistry now requires that key target compounds possess purity of 98% or more. Results here support this requirement and indicate that, in transport and uptake studies, impurity can cause an underestimation in J_{max}, as well as an underestimation in K_t. This impact on apparent K_t appears to be surprising, since impurity would cause the apparent affinity of a substrate to be more potent than its true potency. Results of these simulation studies imply that transport studies results that conclude a drug candidate to be a potent substrate merit inspection, to assure that impurity is not causing over-favorable results, particularly if a chemical reactant, precursor, or side product is known to be a potent inhibitor.

For example, in employing hASBT as a carrier for drug delivery and a bile acid prodrug where TCA (K_i = 5 μM) is the targeting moiety, a result of K_t = 50 μM could reflect several scenarios, such as: 1) the target compound to possess K_t = 50 μM; 2) the target to possess K_t = 500 μM but also be contaminated with a most strong impurity (K_i = 0.05 μM) at a level of X_i = 0.075%; 3) the target to possess K_t = 500 μM but also be contaminated with a very strong impurity (K_i = 0.5 μM) at a level of X_i = 0.8%; or 4) the target to possess K_t = 500 μM but also be contaminated with a impurity (K_i = 5 μM) at a level of X_i = 8%.

Experience to date suggests scenario “1” as most likely, which is favorable as the intent is to measure unbiased parameters, but emphasizes purification methods should be designed to remove critical impurities from target compound. Scenario “2” does not appear likely, as the lowest K_i to date is 0.5μM or about 10-fold less potent that this scenario requires. Scenario “4” is not practically possible, since this scenario would require at least 8% impurity by TCA, which will not occur with purification effort. Scenario “3” represents a potentially real and

challenging situation, where a relatively small amount (i.e. $X_i = 0.8\%$) of most potent impurity (e.g. TLCA with $K_i = 0.5$ μM) contaminates the target. However, formation of TLCA from unreacted taurocholate is not expected. Consideration of these scenarios supports a 97.5% to 98% purity level, as long as very potent impurities are not present. For target compounds of high interest, inhibition data that show a drug candidate to be potent inhibitor merit inspection that impurity is not causing over-favorable results, particularly if a chemical reactant, precursor, or side product is known to be a potent inhibitor.

Results from this study motivates purification methods to eliminate, if not minimize, unreacted bile acid in target bile acid prodrug compounds. Additionally, in the case of conjugates of highly potent bile acids, enough hydrolytic stability must be assured in the transport/inhibition buffer so that regeneration of the parent targeting moiety does not occur during the course of the assay. Unfortunately, target compounds that show moderate or weak affinity cannot be completely excluded from potential bias, as small amounts of very strong impurity can bias results and evade conventional detection. Hence, the ultimate benefit of these findings may be the need for careful consideration of impurity effect on transport and inhibition results, particularly when QSAR analysis cannot explain high compound potency.

In conclusion, the present study concerns two types of ADME transport studies: inhibition studies and transport/uptake studies. Presumably, in a competitive binding study (e.g. inhibition study), impurity with a potency greater than test compound potency may cause test compound to appear more potent than actually is. This expectation was found to be correct here and offers quantitative guidelines. Surprisingly, an expectation that a potent impurity would diminish the apparent potency of a test compound in the uptake assay (i.e. increase Michaelis-Menten K_t) was found here to be incorrect. Rather, potent impurity, which reduces test compound flux, resulted in test compound to appear to possess higher substrate affinity (i.e. exhibit a lower K_t). This study provides quantitative guidelines, which are currently lacking, about maximum impurity levels to avoid bias on transporter parameter estimates (i.e. K_t, J_{max}, and K_i) in early drug develpment. Results have implications for other types of early discover assays, such as pharmacologic binding studies.

Supplementary Material

Refer to Web version on PubMed Central for supplementary material.

Acknowledgments

This work was support in part by National Institutes of Health grants DK67530 (to JEP).

List of Abbreviations

hASBT	human apical sodium-dependent bile acid transporter
SLC	Solute carrier family
MDCK	Madin-Darby canine kidney
HBSS	Hanks balanced salt solution
ABL	aqueous boundary layer
QSAR	quantitative-structure activity relationship
GCA	glycocholic acid
TCA	taurocholic acid
TLCA	taurolithocholic acid

UDCA ursodeoxycholic acid

References

Balakrishnan A, Hussainzada N, Gonzalez P, Bermejo M, Swaan PW, Polli JE. Bias in estimation of transporter kinetic parameters from overexpression systems: Interplay of transporter expression level and substrate affinity. J Pharmacol Exp Ther 2007;320:133–144. [PubMed: 17038509]

Balakrishnan A, Polli JE. Apical sodium dependent bile acid transporter (ASBT, SLC10A2): a potential prodrug target. Mol Pharm 2006;3:223–230. [PubMed: 16749855]

Balakrishnan A, Sussman DJ, Polli JE. Development of stably transfected monolayer overexpressing the human apical sodium-dependent bile acid transporter (hASBT). Pharm Res 2005;22:1269–1280. [PubMed: 16078136]

Balakrishnan A, Wring SA, Coop A, Polli JE. Influence of charge and steric bulk in the C-24 region on the interaction of bile acids with human apical sodium-dependent bile acid transporter. Mol Pharm 2006a;3:282–292. [PubMed: 16749860]

Balakrishnan A, Wring SA, Polli JE. Interaction of native bile acids with human apical sodium-dependent bile acid transporter (hASBT): influence of steroidal hydroxylation pattern and C-24 conjugation. Pharm Res 2006b;23:1451–1459. [PubMed: 16783481]

Buchwald H, Williams SE, Matts JP, Boen JR. Lipid modulation and liver function tests. A report of the Program on the Surgical Control of the Hyperlipidemias (POSCH). J Cardiovasc Risk 2002;9:83–87. [PubMed: 12006915]

Copeland, RA. Enzymes: a practical introduction to structure, mechanism, and data analysis. J. Wiley; New York: 2000.

Hagenbuch B, Dawson P. The sodium bile salt cotransport family SLC10. Pflugers Arch 2004;447:566–570. [PubMed: 12851823]

Hofmann AF. The continuing importance of bile acids in liver and intestinal disease. Arch Intern Med 1999;159:2647–2658. [PubMed: 10597755]

Hofmann AF, Mysels KJ. Bile acid solubility and precipitation in vitro and in vivo: the role of conjugation, pH, and Ca2+ ions. J Lipid Res 1992;33:617–626. [PubMed: 1619357]

Sievanen E. Exploitation of bile acid transport systems in prodrug design. Molecules 2007;12:1859–1889. [PubMed: 17960093]

Tolle-Sander S, Lentz KA, Maeda DY, Coop A, Polli JE. Increased acyclovir oral bioavailability via a bile acid conjugate. Mol Pharm 2004;1:40–48. [PubMed: 15832499]

APPENDIX A

Derivation of Influence of Impurity on Solute Flux

The objective of this appendix is to derive eqn 1, which models the impact of impurity on solute flux in transport studies. For the flux of a solute across a monolayer, where solute is translocated both passively and actively, but where inhibitor is present to inhibit active solute flux,

$$J_{mono}=\frac{J_{\max}\cdot S}{K_t(1+I/K_i)+S}+P_p\cdot S \tag{A1}$$

where J_{mono} is total flux across cell monolayer, S is concentration of solute, I is the concentration of inhibitor, P_p is the passive permeability of solute, K_t and J_{max} are the Michaelis-Menten constants for active transport, and K_i is the inhibitor affinity of I. Inhibitor I is an impurity present in the solute S. Only a single impurity is present. For example, in the design of bile acid conjugates to serve as prodrugs to target hASBT, the bile acid conjugate is

the solute, but can be contaminated with unreacted bile acid, which was a starting material in conjugate synthesis.

The mole fraction impurity in the sample is

$$X_i = \frac{I}{I+S} \tag{A2}$$

where X_i is mole fraction of impurity in the sample.

$$I = \frac{X_i \cdot S}{1 - X_i} \tag{A3}$$

Substituting eqn A3 into eqn A1,

$$J_{mono} = \frac{J_{\max} \cdot S}{K_t\left(1 + \frac{\left(\frac{X_i \cdot S}{1-X_i}\right)}{K_i}\right) + S} + P_p \cdot S \tag{A4}$$

The flux in eqn A4 is the flux across a monolayer where solute is both actively and passively translocated, but where an impurity inhibits active solute transport. It should be emphasized that S is actual solute concentration.

From eqn A4, the monolayer permeability can be considered to be

$$P_{mono} = \frac{J_{\max}}{K_t\left(1 + \frac{\left(\frac{X_i \cdot S}{1-X_i}\right)}{K_i}\right) + S} + P_p \tag{A5}$$

Since flux across a monolayer is in series with the aqueous boundary layer (ABL),

$$\frac{1}{P_{app}} = \frac{1}{P_{ABL}} + \frac{1}{P_{mono}} \tag{A6}$$

where P_{app} is apparent permeability and P_{ABL} is the permeability of S across the ABL.

Substituting eqn A5 into eqn A6,

$$\frac{1}{P_{app}} = \frac{1}{P_{ABL}} + \frac{1}{\frac{J_{\max}}{K_t\left(1 + \frac{\left(\frac{X_i \cdot S}{1-X_i}\right)}{K_i}\right) + S} + P_p} \tag{A7}$$

$$P_{app}=\frac{P_{ABL}\cdot\left(\frac{J_{\max}}{K_t\left(1+\frac{\left(\frac{X_i\cdot S}{1-X_i}\right)}{K_i}\right)+S}+P_p\right)}{P_{ABL}+\frac{J_{\max}}{K_t\left(1+\frac{\left(\frac{X_i\cdot S}{1-X_i}\right)}{K_i}\right)+S}+P_p} \tag{A8}$$

With impurity present in solute, the apparent flux is $J_{X_i}= P_{app}\cdot S$, such that

$$J_{X_i}=\frac{P_{ABL}\cdot\left(\frac{J_{\max}}{K_t\left(1+\frac{\left(\frac{X_i\cdot S}{1-X_i}\right)}{K_i}\right)+S}+P_p\right)}{P_{ABL}+\frac{J_{\max}}{K_t\left(1+\frac{\left(\frac{X_i\cdot S}{1-X_i}\right)}{K_i}\right)+S}+P_p}\cdot S \tag{A9}$$

Eqn A9 describes the flux of a solute across a monolayer, in the presence of an ABL, where solute is translocated actively and passively, and where impurity inhibits solute active transport.

If no impurity is present or if impurity does not inhibit solute active transport, eqn A9 simplifies to

$$J=\frac{P_{ABL}\cdot\left(\frac{J_{\max}}{K_t+S}+P_p\right)}{P_{ABL}+\frac{J_{\max}}{K_t+S}+P_p}\cdot S \tag{A10}$$

Eqn A9 and A10 are eqn 1 and 2 in the Methods section and represent the impurity-present transport model and impurity-absent transport model, respectively.

APPENDIX B

Derivation of Influence of Impurity on Apparent Inhibitor Performance

The objective of this appendix is to derive eqn 4, which models the impact of impurity on apparent inhibitor performance in inhibition studies. This derivation employs a Michalis-Menten approach to the scenario where impurity inhibits transporter function (Copeland, 2000).

Figure 4 represents the inhibition of a transporter E by two mutually exclusive inhibitors I and J_{imp}, where S is a substrate, I is an inhibitor and J_{imp} is an impurity of I which also inhibits E.

$$\text{Let } K_t=\frac{k_{-1}+k_2}{k_1}$$

$$K_i = \frac{k'_{-1} + k'_2}{k'_1}$$

$$K_j = \frac{k''_{-1} + k''_2}{k''_1}$$

where K_t, K_i, and K_j are denoted affinity constants of S, I, and J_{imp} for the transporter.

If $k'_{-1} \gg k'_2$ (i.e. rapid equilibrium),

$$K_i = \frac{k'_{-1}}{k'_1}$$

$$\text{Hence, } K_i = \frac{E \cdot I}{EI}$$

$$EI = \frac{E \cdot I}{K_i} \tag{B1}$$

If $k''_{-1} \gg k''_2$,

$$K_j = \frac{k''_{-1}}{k''_1}$$

$$\text{Hence, } K_j = \frac{E \cdot J_{imp}}{EJ_{imp}}$$

$$EJ_{imp} = \frac{E \cdot J_{imp}}{K_j} \tag{B2}$$

The rate of translocation of substrate S is

$$j_2 = k_2 ES \tag{B3}$$

and the total concentration of transporter at any time is

$$E_t = E + ES + EI + EJ_{imp} \tag{B4}$$

Dividing eqn B3 by eqn B4

$$\frac{j}{E_t} = \frac{k_2 ES}{E + ES + EI + EJ_{imp}} \tag{B5}$$

$$j = \frac{J_{\max} \cdot ES}{E + ES + EI + EJ_{imp}} \tag{B6}$$

Where $J_{max} = k_2 \cdot E_t$ is the maximum flux when transporter is saturated.

At steady state,

$$dES/dt = k_1 E \cdot S - (k_{-1} ES + k_p ES) = 0 \tag{B7}$$

$$\text{Hence, } ES = \frac{k_1 E \cdot S}{k_{-1} + k_2} \tag{B8}$$

Substituting K_t into eqn B8,

$$ES = \frac{E \cdot S}{K_t} \tag{B9}$$

Substituting eqn B1, B2, and B9 into eqn B6,

$$J = \frac{J_{\max} \frac{E \cdot S}{K_t}}{E + \frac{E \cdot S}{K_t} + \frac{E \cdot I}{K_i} + \frac{E \cdot J_{imp}}{K_j}} = \frac{J_{\max} \frac{S}{K_t}}{1 + \frac{S}{K_t} + \frac{I}{K_i} + \frac{J_{imp}}{K_j}}$$

$$J = \frac{J_{\max} S}{K_t \left(1 + \frac{I}{K_i} + \frac{J_{imp}}{K_j}\right) + S} \tag{B10}$$

which expresses the rate of translocation of substrate S by a transporter in presence of two mutually exclusive inhibitors.

Allowing passive flux of solute across a monolayer, eqn B10 yields

$$J=\frac{J_{\max}S}{K_t\left(1+\frac{I}{K_i}+\frac{J_{imp}}{K_j}\right)+S}+P_p\cdot S \tag{B11}$$

where Pp is the passive permeability of solute across the monolayer.

Let $X_j=\frac{J_{imp}}{J_{imp}+I}$ be the mole fraction of inhibitor J_{imp} contaminating inhibitor I. For example, I is a prodrug synthesized by conjugation of a bile acid and a drug, J_{imp} is an impurity (e.g. unreacted bile acid) that is also an inhibitor of hASBT.

$$J_{imp}=\frac{X_j\cdot I}{1-X_j} \tag{B12}$$

Substituting eqn B12 into eqn B11 and considering the presence of an ABL (Appendix A),

$$J_{X_j}=\frac{P_{ABL}\cdot\left(\frac{J_{\max}}{K_t\left(1+\frac{I}{K_i}+\frac{\left(\frac{X_j\cdot I}{1-X_j}\right)}{K_j}\right)+S}+P_p\right)}{P_{ABL}+\frac{J_{\max}}{K_t\left(1+\frac{I}{K_i}+\frac{\left(\frac{X_j\cdot I}{1-X_j}\right)}{K_j}\right)+S}+P_p}\cdot S \tag{B13}$$

where is J_{Xj} is the total flux of a solute S (both active and passive) in presence of two inhibitors when an ABL is considered.

If impurity J_{imp} is not present or if does not inhibit the transporter, eqn B13 simplifies to

$$J=\frac{P_{ABL}\cdot\left(\frac{J_{\max}}{K_t\left(1+\frac{I}{K_i}\right)+S}+P_p\right)}{P_{ABL}+\frac{J_{\max}}{K_t\left(1+\frac{I}{K_i}\right)+S}+P_p}\cdot S \tag{B14}$$

Eqn B13 and B14 are eqn 3 and 4 in the Experimenal Section and represent the impurity-present inhibition model and impurity-absent inhibition model, respectively.

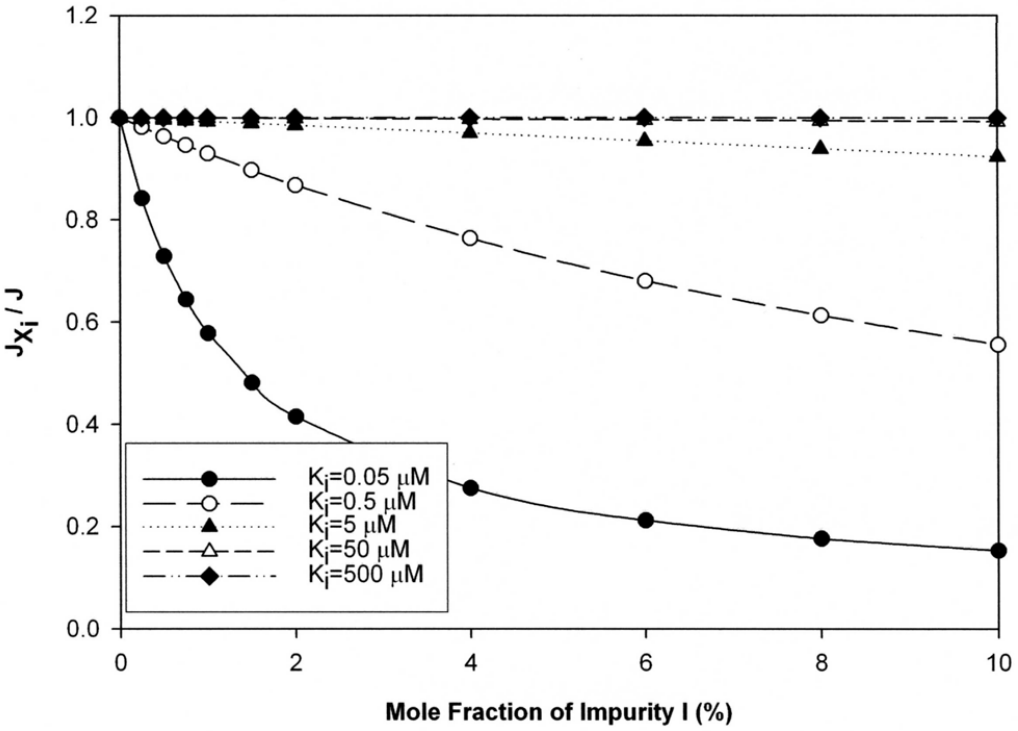

Figure 1. Decrease in total flux of substrate across a monolayer due to presence of impurity

Total flux of a substrate (J) was simulated using eqn 2 (i.e. impurity-absent model) for K_t level of 50 μM. Equation 1 (i.e. impurity-present model) modeled the influence of impurity on substrate total flux (J_{Xi}). When impurity present, X_i varied from 0 to 10 %, over five different levels of K_i (0.05, 0.5, 5, 50, and 500 μM respectively). impurity effect was assessed by the ratio of fluxes in the presence and absence of impurity (i.e. ratio of J_{Xi} versus J). The ratio J_{Xi}/J is 1 when no impurity is present and then decreases consistently as impurity level increased. The drop in total flux was more dramatic as the potency of the inhibitor increased.

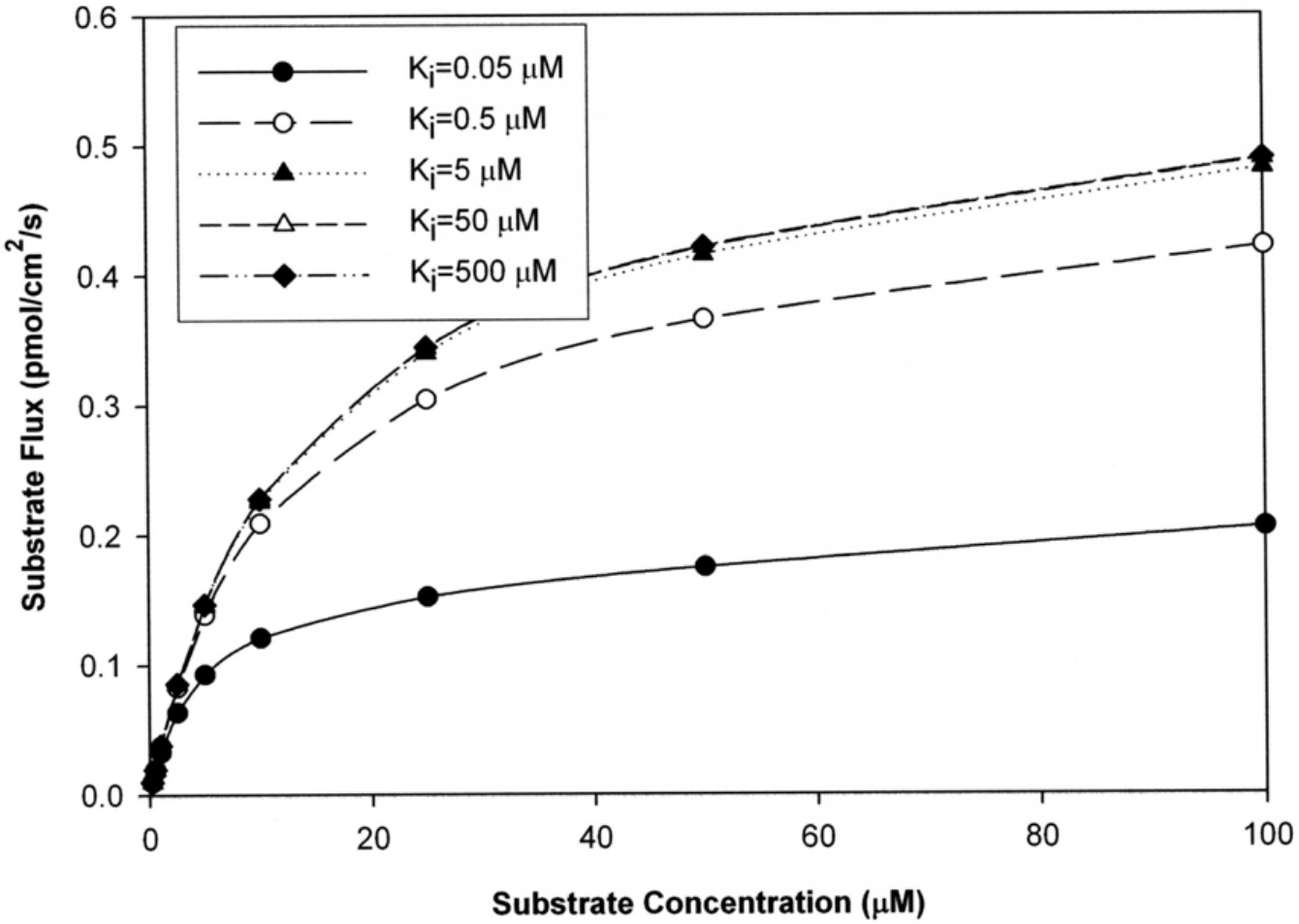

Figure 2. Flux profile of a substrate with K_t of 5 μM in presence of 2% mole fraction impurity

Simulations were performed where K_i values of impurity varied from 0.05 to 500 μM. The total flux of substrate decreased with impurity potency. Apparent J_{max} and apparent K_t both also decreased with impurity potency. For example, when the impurity K_i was 5 μM, apparent J_{max} and apparent K_t were 0.48 pmol/cm^2/s and 12 μM respectively. However, when K_i was 0.05 μM, apparent J_{max} and apparent K_t were both 2.5-fold lower than these values.

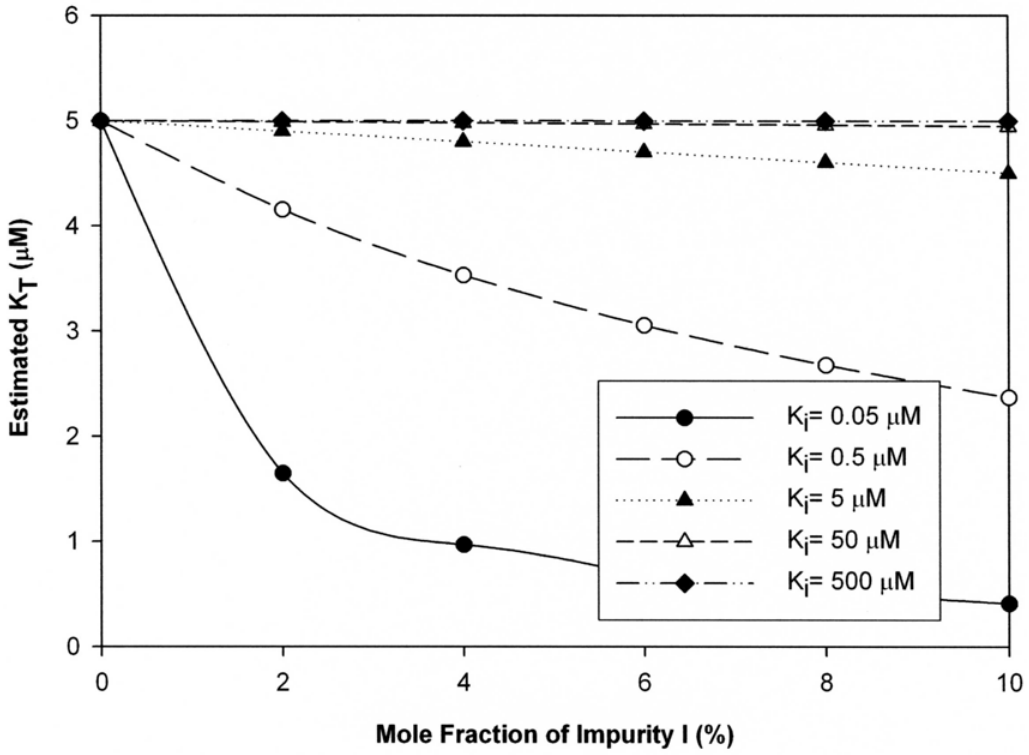

Figure 3. Impact of impurity on K_t estimates from transport studies when impurity not considered

K_t value was 5 μM. The mole fraction of impurity X_i varied from 0 to 10 %. K_i values were 0.05 (filled circle), 0.5 (open circle), 5 (filled triangle), 50 (open triangle), or 500 μM (filled diamond). Impurity generally reduced estimated K_t. An estimated K_t of 80% or less than the "true K_t" value was considered unacceptably biased. Impurity level and inhibitory potency each promoted bias. Bias in K_t estimates was increasingly sensitive to impurity level when "true K_t" was at least 10-fold larger than K_i, and was very large when K_t while K_i was strong. Interestingly, analogous plots for bias in J_{max} followed identical trends (supplemental data).

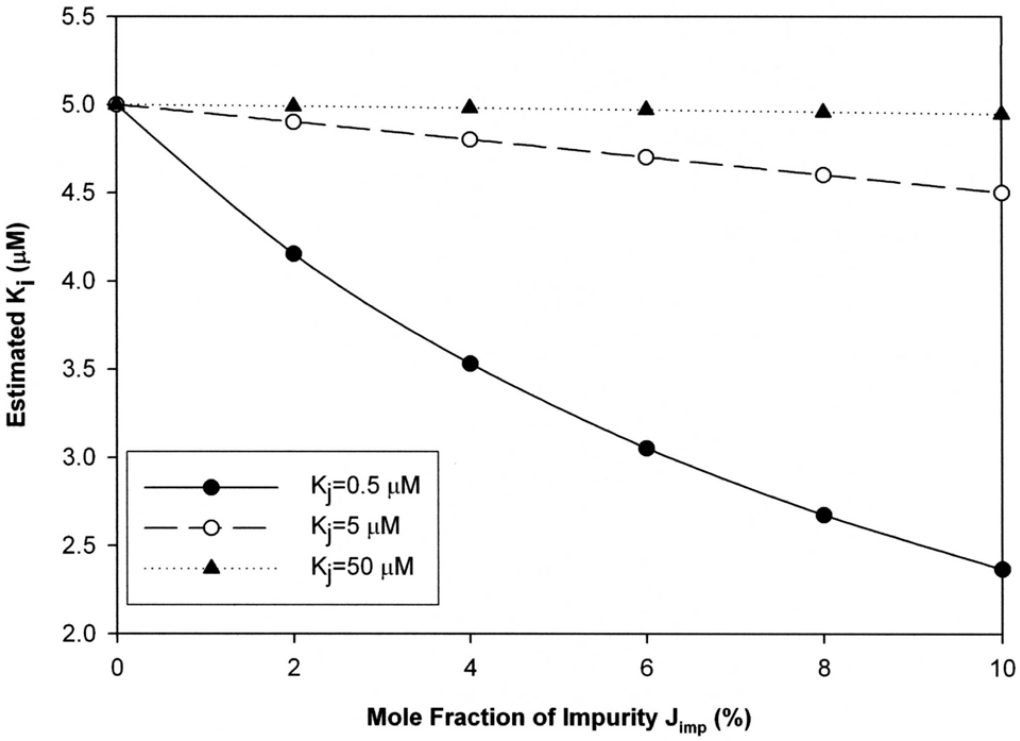

Figure 4. Impact of impurity on K_i estimate from inhibition studies when inhibitor contaminated with impurity

K_i is inhibition constant of inhibitor. K_j is inhibition constant of impurity. Impurity contaminated the inhibitor. "True K_i" value was 5 μM. Impurity level was varied from 0 to 10% mole fraction. K_j was 0.5 (filled circle), 5 (open circle) and 50 μM (filled triangle), respectively. Impurity generally resulted in either no effect or decreased apparent K_i. An estimated K_i of 80% or less than the "true K_i" was considered unacceptably biased. When present, bias was always negative (i.e. estimated K_i less than "true K_i"). No bias in K_i estimate was observed when the ratio K_i/K_j is 1 or less. However, K_i/K_j ratios of 10 or higher caused K_i bias when impurity level exceeded 2.5%. No fit was obtained for K_i 500 μM (data not shown).

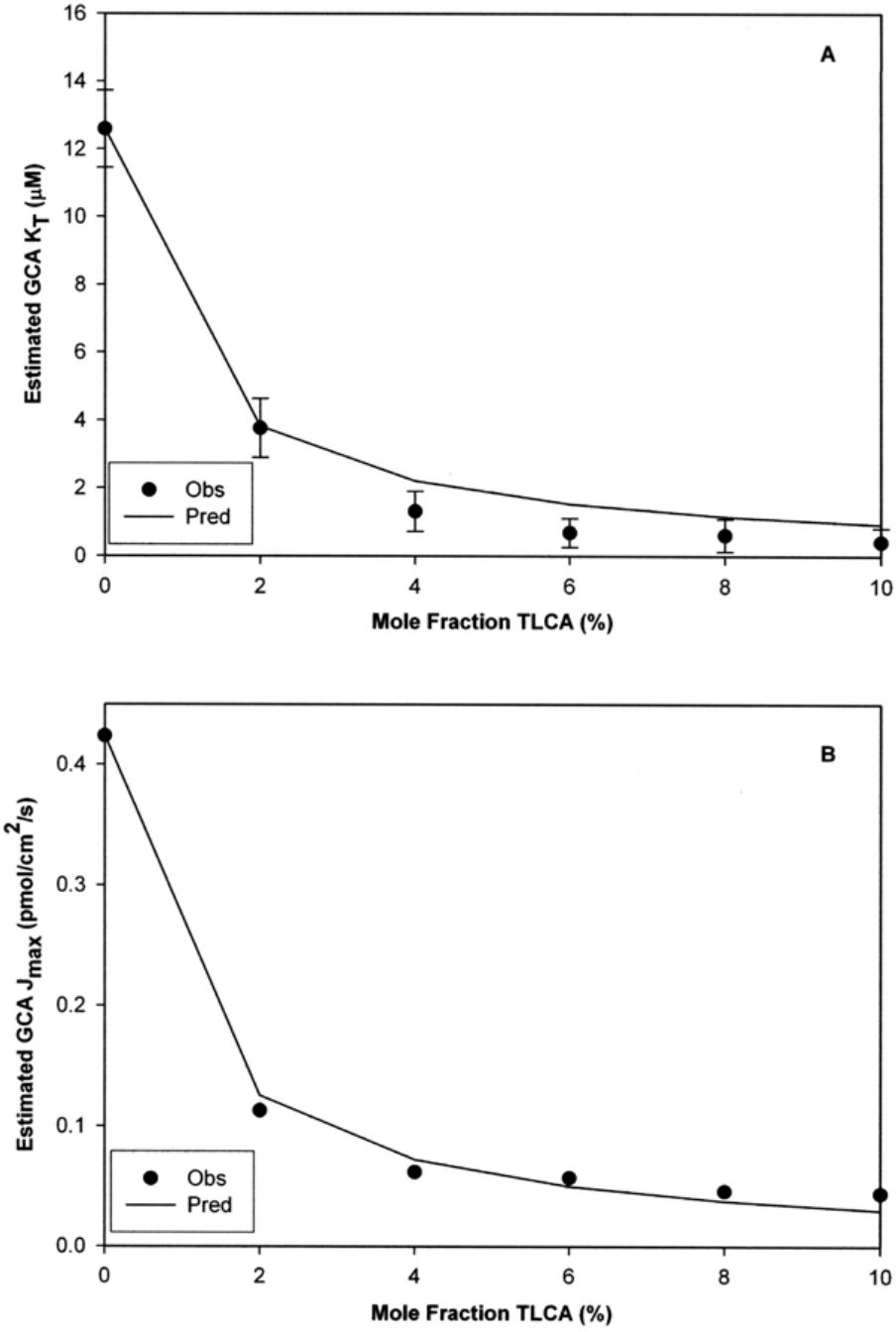

Figure 5. Impact of taurolithocholate on glycocholate kinetic estimates from uptake studies

Mole fraction of TLCA was varied from 0 to 10%. TLCA contamination produced negative bias on GCA kinetic estimates (i.e. increased "apparent" affinity and decreased "apparent" capacity in panels A and B, respectively). A 2% mole fraction of TLCA generated approximately 70% error on the estimation of both GCA K_t and J_{max}. These experimental observations followed the model predicted trends. Unbiased K_t and J_{max} of substrate were 12.6 (±1.1) μM and 0.424 (±0.041) pmol/cm^2/s, while TLCA K_i was 0.11 (±0.01) μM. Data are presented as mean (±S.E.M.). (S.E.M. bars smaller than symbol in panel B).

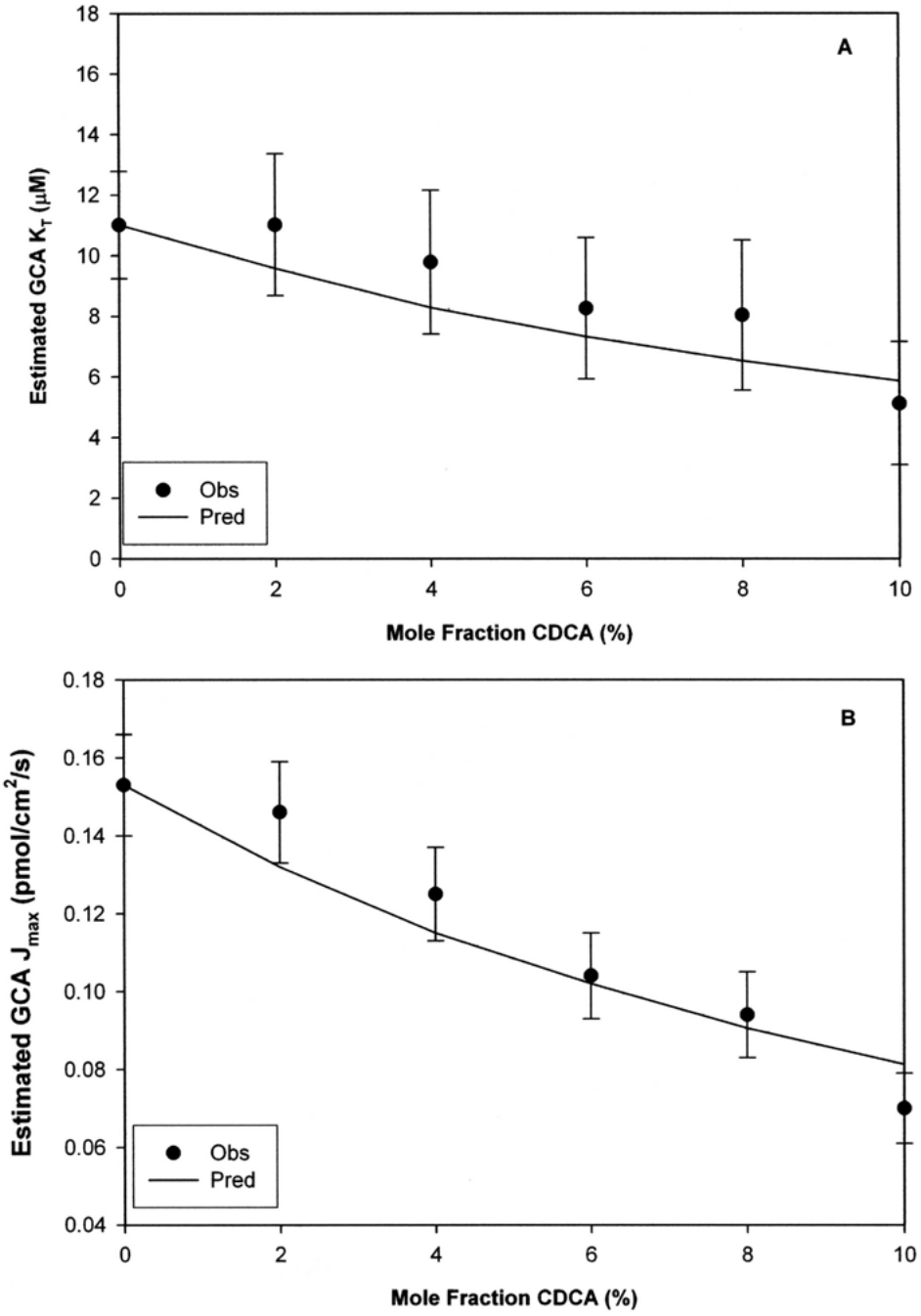

Figure 6. Impact of chenodeoxycholate on glycocholate kinetic estimates from uptake studies

Experimentally CDCA contamination produced modest negative bias on GCA K_t (panel A) and GCA J_{max} (panel B), particularly compared to the larger bias shown in Fig 7. This more modest level of bias reflects CDCA impurity is less potent than TLCA impurity in Fig 7. However, even a 10% mole fraction of CDCA impurity caused 50% bias in estimated GCA K_t and J_{max} (Fig 8 panels A and B, respectively). Unbiased K_t and J_{max} of GCA substrate were 11.0 (±1.8) μM and 0.153 (±0.013) pmol/cm^2/s, while CDCA K_i was 1.39 (±0.39) μM. Data are presented as mean (±S.E.M.).

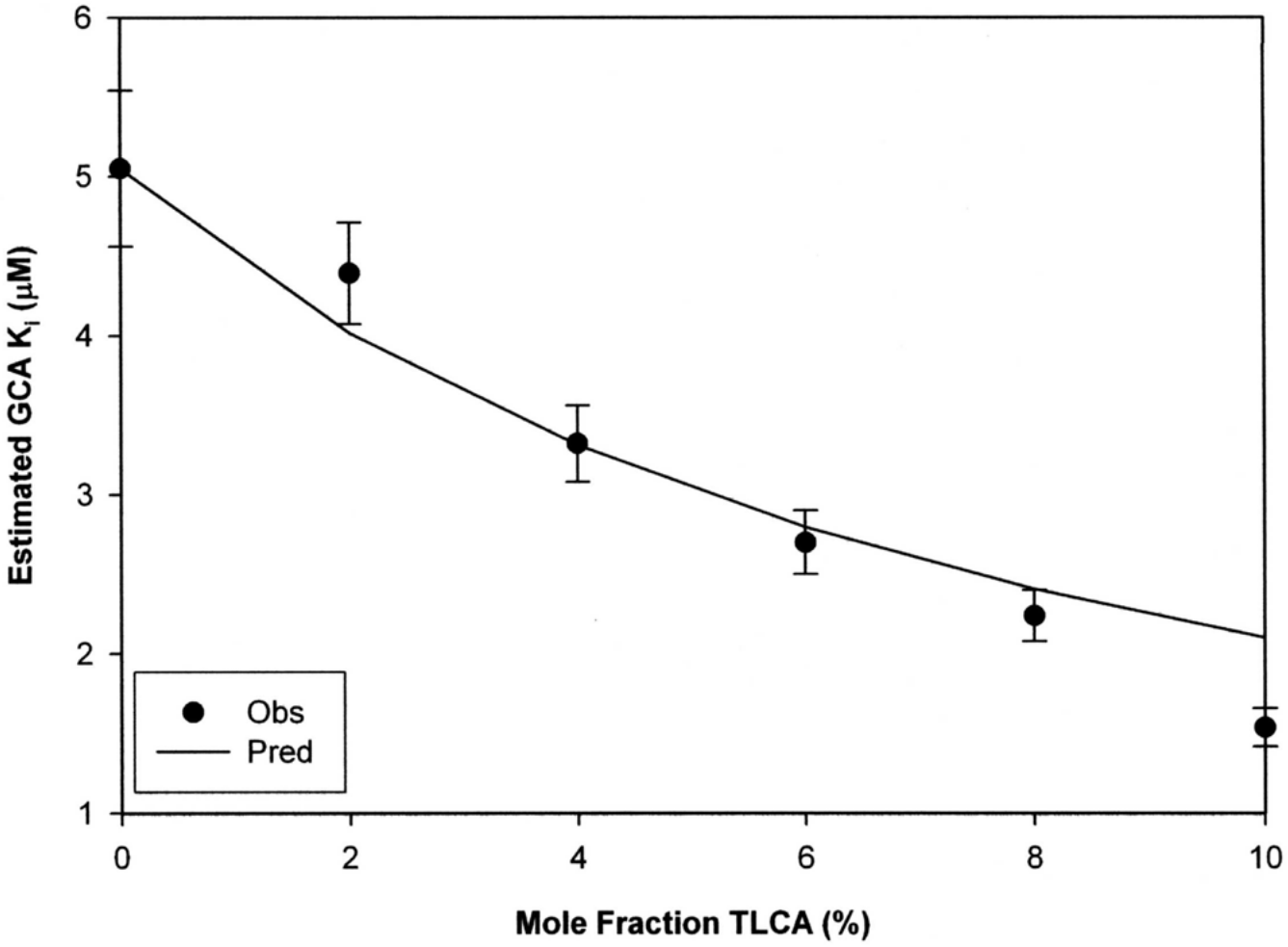

Figure 7. Impact of taurolithocholate on glycocholate K_i when taurolithocholate was present as impurity

TLCA contamination produced negative bias on GCA "apparent" affinity. The 4% mole fraction of TLCA caused 34% error in GCA K_i estimation. Predicted bias anticipated these experimental observations. Unbiased K_i of GCA was 5.05 (±0.48) μM, while TLCA K_j was 0.40 (±0.04) μM. Data are presented as mean (±S.E.M.).

Table 1

Experimental design.

Simulation/Experiment	Type of study	Substrate K_t (μM)	Inhibitor K_i (μM)	Impurity K_i (μM)
Simulation	Transport/uptake	5, 50, 500	none	K_i = 0.05–500
Experiment	Uptake	GCA ($K_t \approx 11$)	none	TLCA (K_i = 0.11) CDCA (K_i = 1.39) UDCA (K_i = 24.2)
Simulation	Inhibition	5	0.05–50	K_j = 0.5–50
Experiment	Inhibition	TCA (K_t = 5.03)	GCA (K_i = 5.05)	TLCA (K_j = 0.40)

Table 2

Necessary impurity level to cause 20% bias on K_t estimates from transport studies.

Potency of substrate	K_t/K_i[a]	Necessary X_i level to cause bias in K_t
Strong (K_t = 5 μM)	≤ 1	Never a concern when $X_i \leq 10\%$
	10	≥ 2.5%
	100	≥ 0.5%
Moderate (K_t = 50 μM)	≤ 1	Never a concern when $X_i \leq 10\%$
	10	≥ 2.5%
	100	≥ 0.25%
	1000	≥ 0.1%
Weak (K_t = 500 μM)	≤ 1	Never a concern when $X_i \leq 10\%$
	10	> 2.5%
	100	≥ 0.25%
	1000	Trace
	10000	Trace

[a] K_t/K_i reflects the ratio of the "true" affinity constant of the substrate of interest versus the inhibition constant of its impurity.

Table 3

Necessary impurity level to cause 20% bias on K_i estimates from inhibition studies.

Potency of Inhibitor	K_i/K_j[a]	Necessary X_j level to cause bias in K_i
Most strong (K_i = 0.05 μM)	≤ 0.1	Never a concern when $X_j \leq 10\%$
Very strong (K_i = 0.5 μM)	≤ 1	Never a concern when $X_j \leq 10\%$
Strong (K_i = 5 μM)	≤ 1	Never a concern when $X_j \leq 10\%$
	10	2.5%
Moderate (K_i = 50 μM)	≤ 1	Never a concern When $X_j < 10\%$
	10	≥ 2.5%
	100	≥ 0.6%
Weak (K_i = 500 μM)	Eqn 4 (appendix B) did not adequately fit data.	

[a] K_i/K_j reflects the ratio of the "true" inhibition constant of the inhibitor of interest versus the inhibition constant of its impurity.